Ice Sticks – Ice Adhesion for Locomotion on Icy Surfaces

Mooijman, Thomas; Meersman, Marnix; Cazaux, Stéphanie; Jovanova, Jovana

DOI
10.1115/SMASIS2025-167744

Publication date
2025

Document Version
Final published version

Published in
Proceedings of ASME 2025 Conference on Smart Materials, Adaptive Structures and Intelligent Systems, SMASIS 2025

Citation (APA)
Mooijman, T., Meersman, M., Cazaux, S., & Jovanova, J. (2025). Ice Sticks – Ice Adhesion for Locomotion on Icy Surfaces. In *Proceedings of ASME 2025 Conference on Smart Materials, Adaptive Structures and Intelligent Systems, SMASIS 2025* Article V001T06A005 American Society of Mechanical Engineers (ASME). https://doi.org/10.1115/SMASIS2025-167744

Proceedings of the ASME 2025 Conference on Smart Materials,
Adaptive Structures and Intelligent Systems
SMASIS2025
September 8-10, 2025, St. Louis, MO

SMASIS2025-167744

ICE STICKS – ICE ADHESION FOR LOCOMOTION ON ICY SURFACES

Thomas Mooijman[1], Marnix Meersman[2], Stéphanie Cazaux[2,3,*], Jovana Jovanova[1]

[1]Faculty of Mechanical Engineering, Delft University of Technology, 2628 CD Delft, The Netherlands
[2]Faculty of Aerospace Engineering, Delft University of Technology, 2629 HS Delft, The Netherlands
[3]Leiden Observatory, Leiden University, 2300 RA Leiden, The Netherlands

ABSTRACT

Enceladus, one of Saturn's icy moons, has been a subject of intense scientific interest since the Cassini mission revealed a subsurface ocean containing salts and complex organic molecules. This ocean, buried beneath kilometers of ice, is accessible only through surface cracks at the moon's south pole, where geysers emerge. In support of future missions searching for extraterrestrial life within our solar system, we developed a robot aimed at exploring such environments. Using Peltier elements, the robot attaches to icy surfaces by locally melting and refreezing water and detaches by re-melting the contact area. Adhesion tests based on local phase change dynamics demonstrate strong bonding, often exceeding the cohesive strength of the ice. While originally developed for planetary exploration, the underlying principle is also applicable to Earth-based operations such as exploration and rescue missions in icy environments.

Keywords: Ice Climbing Robot, Ice adhesion, Bio-Inspired Robotics, Planetary Exploration, Icy Moons

1. INTRODUCTION

The Cassini-Huygens spacecraft completed its exploration of the Saturn system in 2017 after 20 years of research on the planet and its moons. One of its most remarkable discoveries was the detection of cryovolcanic plumes on Saturn's small moon Enceladus, which eject gas and icy grains into space from a subsurface ocean [1]. Cassini flew through these plumes on multiple occasions to analyze their composition [2], identifying a variety of molecules, including salts, volatiles, and complex organic compounds [3], which are believed to reflect the composition of the underlying ocean. These findings have made Enceladus a key focus in the search for extraterrestrial life [2], and icy moon exploration has since become a priority for both NASA and ESA. In recent years, numerous scientific missions have been proposed to return to Enceladus [4–7] or to investigate other icy moons [8], with the aim of determining whether these environments could host life.

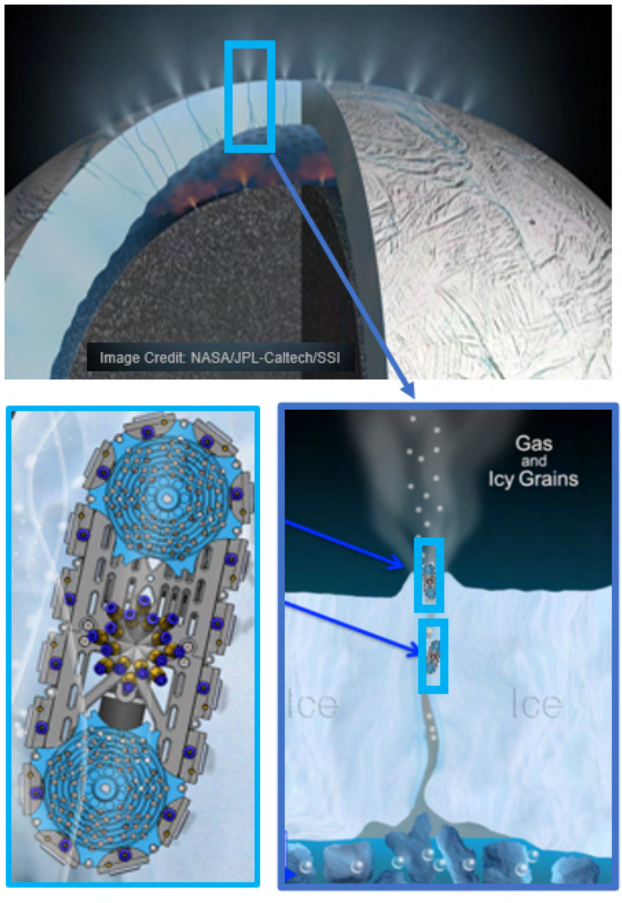

FIGURE 1: CONCEPTUAL DESIGN OF ICE CLIMBING ROBOT IN ENCELADUS' TIGER STRIPES.

*Corresponding author: s.m.cazaux@tudelft.nl
Documentation for `asmeconf.cls`: Version 1.41, June 21, 2025.

The large plumes of water vapor ejected from Enceladus' South Polar Terrain indicate a substantial subsurface reservoir, where water beneath the thick ice crust is maintained at approximately 273 K. These plumes are expelled at high velocities, and due to the moon's low atmospheric pressure and gravity (0.113 $m \cdot s^{-2}$), they extend far above the surface [9]. As the South Polar Region is of particular interest for future exploration missions [5, 6, 10], the scale of surface features is highly relevant for both potential landing strategies and mobility design. The so-called "Tiger Stripes" refer to V-shaped valleys flanked by nearly parallel ridges [11]. The ridges are estimated to rise 100–150 m above the terrain, with valleys ranging from 200–250 m deep and spanning a total width of 2–5 km.

Realizing a landed life-detection mission to Enceladus that can explore the south polar cracks presents a significant challenge. The extreme and largely unknown environment demands a robust, versatile, autonomous, and adaptable robot capable of navigating harsh terrain while carrying a scientific payload for life detection. Current exploration proposals include melting probes [4, 5, 8], snake-like robots designed to crawl through icy crevasses [10]. However, these systems face limitations related to mechanical complexity, energy consumption, and scalability.

Only one ice wall-climbing robot has been proposed for exploring icy moons: the IceWorm robot developed by NASA [12]. This system employs two motorized alpinist screws, similar to those used by human ice climbers to create anchor points. While this system is capable of scaling individual ice walls, its mechanical anchoring method is energy-intensive and induces high stress on ice walls, whose mechanical properties remain poorly understood at the extremely low temperatures and pressures found in such environments.

In this work, we propose a different design approach, one that uses the environmental challenges to the robot's functional advantage. Specifically, we exploit the adhesive properties of ice as part of the locomotion strategy, enabling the robot to stick and move across icy surfaces wherever ice is present. On icy moons, the robot could use existing cracks to descend toward the subsurface ocean and collect water samples in the search for life. Our concept is illustrated in Fig. 1.

A robot capable of moving on icy surfaces would also offer valuable benefits in Earth-based environments. From rescue missions in ice caves to remote exploration in Antarctica, a robot that can maintain secure contact with ice could access difficult-to-reach locations and support ongoing operations. Icy surfaces are prevalent in regions near the North and South Poles, as well as in high-altitude areas across continents. These environments are typically remote and challenging for humans to navigate, yet they hold importance for scientific exploration, logistics, and even sport activities. Ice-climbing robots could provide safer access to such regions and help unlock their potential. Additionally, in urban areas affected by extreme cold, first responders could benefit from robots capable of traversing icy terrain to reach people in need more quickly and effectively.

In this work, we demonstrate the feasibility of a switchable ice adhesion actuator by designing its components and testing their performance in a cold chamber. The actuator is then integrated as a link within a track-based locomotion system capable of attaching to and detaching from icy surfaces by locally freezing and melting the interface.

2. ADHESION MATERIALS AND EXPERIMENTAL SETUP

2.1. Ice Adhesion

Ice adhesion has been widely studied for decades, although most research focuses on minimizing adhesion strength for de-icing applications rather than maximizing it. At the molecular level, several mechanisms contribute to ice adhesion, including electrostatic interactions, van der Waals forces, and covalent chemical bonding, in descending order of significance [13]. On a macroscopic scale, surface roughness greatly influences ice adhesion strength; while smooth hydrophobic surfaces yield low adhesion, structured (super)hydrophilic and (super)hydrophobic surfaces both exhibit high adhesion due to mechanical interlocking from freezing-induced transitions from Cassie-Baxter to Wenzel wetting states [14]. This indicates the critical role of interlocking effects in ice adhesion phenomena, as illustrated in figure 2a.

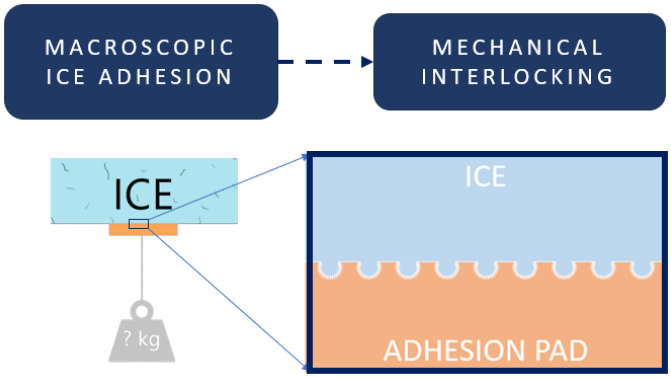

a) Mechanical interlocking effect in ice adhesion

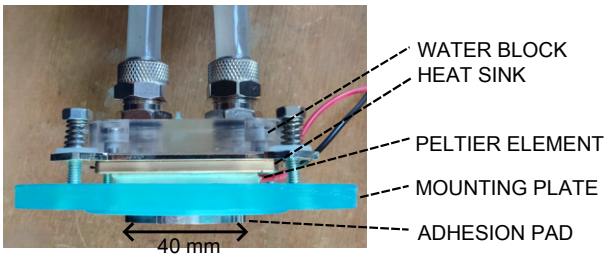

b) Components of the ice adhesion effector

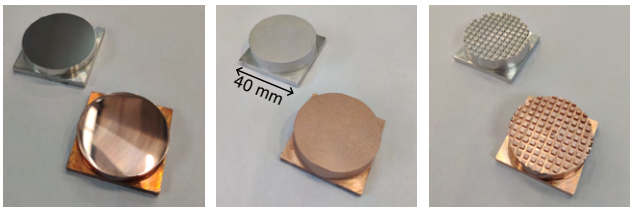

c) 6061 Aluminium and copper adhesion pads: (left) Polished (4000K), (middle) grit blasted, (right) protruding grid pattern

FIGURE 2: TOP PANEL: PRINCIPLE OF INTERLOCKING USED FOR THE ADHESION MECHANISM. MIDDLE PANEL: ADHESION END EFFECTOR COMPONENTS. BOTTOM PANEL: ADHESION PADS OF DIFFERENT MATERIAL AND SURFACE FINISH.

2.2. Ice Adhesion Effector Design

The ice adhesion effector consists of three main components: the adhesion pad, a Peltier element, and a heat sink. The adhesion pad contacts the ice to form an adhesive connection and must be made from materials suited to this purpose. First, a high surface energy is desirable, as it leads to stronger intermolecular forces, promoting wettability and therefore, intrinsic ice adhesion strength between the substrate (adhesion pad) and ice [15]. Second, because the pad undergoes frequent heating and cooling to trigger local phase changes in the ice, the material should exhibit high thermal diffusivity to respond quickly to changes in temperature.

Based on these criteria, copper and 6061 aluminum were selected as pad materials. Each was fabricated with three different surface treatments: polished to 4000 grit finish, grit-blasted, and machined with a 1 mm-deep grid pattern, resulting in six different adhesion pad configurations. These surface treatments introduce increasing surface roughness to explore the effects of contact area and interlocking on adhesion strength. The pads have outer dimensions of 40 mm × 40 mm × 14 mm, with a projected circular contact area of 1256 mm^2. The grid pattern is milled into the surface of the adhesion pads to a depth of 1 mm using a horizontal milling machine with a 1.5 mm HSS end mill cutter. The grooves are spaced 3.5 mm apart and intersect at 90°, forming a grid-like texture. This surface treatment results in an increased effective contact area of 2125.2 mm^2, representing approximately a 69% increase in surface area compared to the other two treatments.

The Peltier elements are thermally coupled to the adhesion pads using conductive paste to ensure efficient heat transfer. TEC1-12706 modules were used, capable of a maximum cooling power of 65 W and a theoretical maximum temperature difference of 70 K (in the absence of heat flow). Polarity control enables both heating and cooling modes, powered by a constant-current source (1–5 A).

On the opposite side of the Peltier element, a heat sink dissipates both pumped and internal heat. Because cooling performance depends on how effectively heat is removed from the hot side, a liquid cooling system was implemented. A copper water block circulates coolant at 18°C through the heat sink. The complete effector assembly is housed in an additively manufactured enclosure. Figure 2b shows the assembled stack with the housing cover removed.

2.3. Thermal Performance Testing

The thermal performance of the effector was characterized by measuring the temperature response of copper and aluminum adhesion pads. In these tests, the Peltier element was powered with 3 A at 8 V to cool the pads from an ambient temperature of 18°C. Temperature was recorded using a digital sensor mounted on the outer surface of each pad. Results (Figure 3) show that the aluminum pad reached 0°C in 42.9 s, while the copper pad required 53.7 s.

In operation, part of the thermal energy from the Peltier is used to locally melt the ice, not just to cool the pad. This phase change improves overall cooling efficiency by dissipating energy into the ice. To quantify this behavior, we measured the time required to achieve adhesion when the pads were placed directly

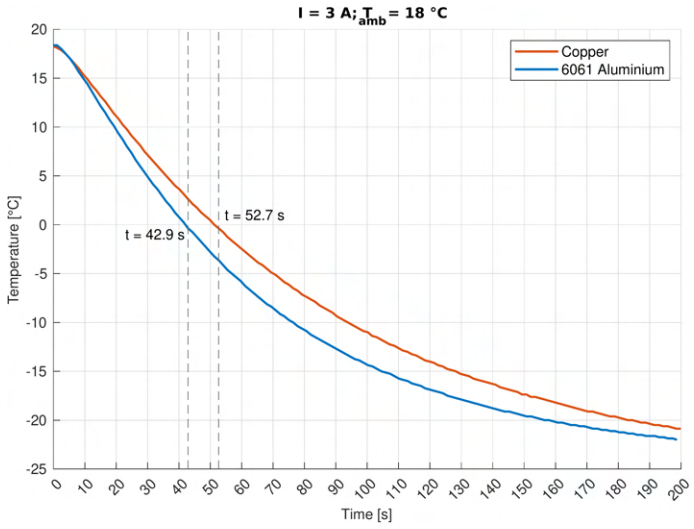

FIGURE 3: TEMPERATURE RESPONSE OF COPPER AND ALUMINUM ADHESION PADS WITH POLISHED SURFACE FINISH UNDER IDENTICAL COOLING CONDITIONS.

on a block of ice (defined as "time-to-adhere"). Adhesion was initiated by powering the Peltier element the moment the pad contacted the ice. The measured time-to-adhere for the copper adhesion pad with a polished surface finish is ~8.5 s and ~6.8 s for the aluminum adhesion pad with identical surface finish.

Although copper has a higher thermal diffusivity, aluminum's lower volumetric heat capacity (about 39% lower) leads to a faster cooling response under these conditions. This effect is evident in both the temperature response (figure 3) and the reduced time-to-adhere. Meanwhile, the surface finish was found to have no effect on the cooling response or the time to adhere.

2.4. Ice Adhesion Strength Experiments

The adhesion strength of the ice effector was quantified using tensile pull-off tests performed with a Zwick Roell Z100 materials testing machine. The tests were conducted inside a cold chamber set to a constant temperature of −15°C. The test setup is shown in Figure 4.

Ice samples were prepared in stainless steel cups (80 mm diameter, 60 mm height) filled with boiled tap water. The water was pre-boiled to reduce dissolved gases and impurities, then frozen using a directional freezing technique to force contaminants toward the base. This ensured that the upper portion of each ice sample was clear and free of defects. Although ice on Enceladus is expected to contain fractures, voids, and volatiles, using clear ice provides a controlled basis for comparing adhesion under ideal conditions.

For each test, the effector was brought into contact with the ice sample. The Peltier element was activated to melt a thin layer of ice, which was then refrozen to establish an adhesive bond. Once the adhesion pad reached −15°C, the machine applied an upward force at a constant rate of 100 µm/s until failure was detected. This test was repeated with six new ice samples.

FIGURE 4: TENSILE PULL-OFF TEST SETUP USED TO MEASURE ADHESION STRENGTH AT −15°C.

2.5. Adhesion Performance Results

The results from the adhesion pull tests, presented in Table 1, show that copper and aluminum exhibit similar adhesion strengths across all surface treatments. Among the surface finishes, grit-blasted pads achieved slightly higher adhesion strength on average. In most tests, failure occurred through a predominantly cohesive fracture of the ice rather than detachment at the interface, indicating that the cohesive strength of ice is the limiting factor in this adhesion method.

TABLE 1: MEAN ICE ADHESION STRENGTH FOR THE SIX ADHESION PADS, EACH TESTED WITH SIX ICE SAMPLES, INCLUDING STANDARD DEVIATION.

Surface Type	Material	Mean adhesion strength [MPa]	Std Dev [MPa (%)]
Polished K4000	Copper	1.220	±0.299 (24.5%)
	Aluminium	1.261	±0.253 (20.1%)
Grit-blasted	Copper	1.348	±0.589 (43.7%)
	Aluminium	1.515	±0.239 (15.8%)
Grid Pattern	Copper	1.026	±0.158 (15.4%)
	Aluminium	1.043	±0.218 (20.1%)

Considering both the thermal response and material density, aluminum was selected for the implementation of the switchable ice adhesion effector. This material will be used in the final design integrated into the robotic system.

3. ROBOT DESIGN AND CONTROL ARCHITECTURE

While mechanical interlocking through ice adhesion was successfully demonstrated at the component level, the next challenge was to achieve continuous locomotion using a discrete adhesion system. Tracked locomotion offers a viable solution for this purpose. Due to their extensive contact area, track systems are well-suited for navigating rough and uneven terrain—conditions likely encountered on icy planetary surfaces.

3.1. Track-Based Locomotion Strategy

Several properties make tracked locomotion especially compatible with ice adhesion robotics. First, the movement relies on zero-velocity contact points with the surface, allowing the vehicle body to advance while maintaining firm anchor points. Second, the modularity of a track system enables the integration of multiple small adhesion effectors into individual links, resulting in continuous climbing or crawling capability, as illustrated in figure 5.

The proposed design consists of a single-track robotic platform with switchable ice adhesion effectors embedded in the track links. The track is composed of multiple links connected via one-degree-of-freedom (1-DOF) passive joints and is driven by a single sprocket. By individually actuating the adhesion state of each link, the robot can generate rigid anchor points for climbing. While the 1-DOF design limits the robot's ability to turn, the primary objective is to demonstrate a proof of concept for ice wall climbing using adhesion-based locomotion.

This modular system allows for flexible configurations. Identical track links can be assembled into various layouts, including single-track or dual-track arrangements. The number of links per track can be adapted to mission-specific requirements such as desired track length or payload capacity.

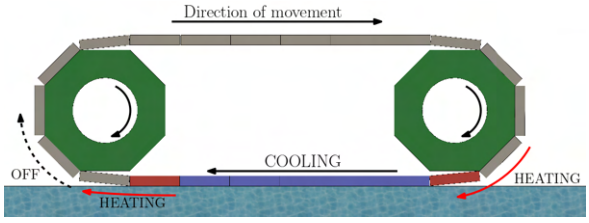

FIGURE 5: LOCOMOTION PRINCIPLE OF TURNING DISCRETE ADHESION SYSTEM INTO CONTINUOUS TRACK MOVEMENT.

3.1.1. Robot Frame and Components The first prototype of the ice-climbing robot was developed with several key design requirements in mind. First, the total mass was limited to a maximum of 5 kg to ensure the system remains compact and resource-efficient. Second, the liquid cooling system, an essential component for ice adhesion effector, needed to be integrated entirely within the robot's structure. This requirement stems from the reliance on the thermoelectric effect to switch adhesion states; successful miniaturization of the cooling system is crucial for the feasibility of the overall design.

In addition, the robot was required to support its own weight, including the cooling loop, using only the integrated ice adhesion actuators. The system is designed to operate in ambient temperatures as low as −15°C. The track consists of 16 modular links, supported by four sprockets—two for driving and two for tensioning. These components are mounted around a central

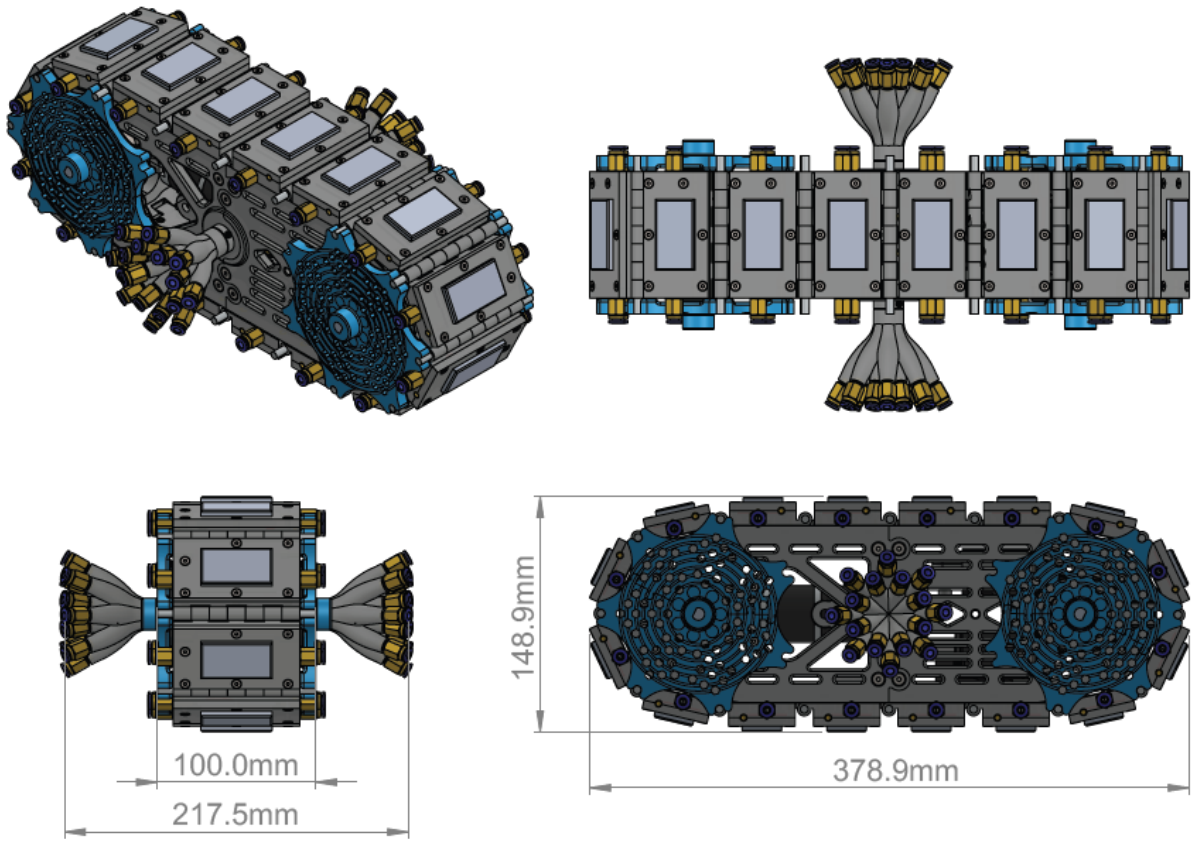

FIGURE 6: 3D CAD MODEL VIEWS OF THE TRACKED LOCOMOTION ICE ADHESION ROBOT.

frame, which houses all systems for locomotion, control, and heat management. The total mass of the robot, including the water within the cooling loop, is 4.2 kg. The complete CAD model of the robot is shown in figure 6.

3.1.2. Liquid Cooling System The frame contains a closed-loop water circulation system that distributes coolant to all track links. The heat absorbed from the Peltier elements must be dissipated to maintain cooling performance. For this purpose, the robot includes an onboard cooling unit consisting of a Laing DDC-1T water pump, a 60 mm radiator, and a 12 VDC axial fan. Together, these elements provide forced air convection through the radiator fins to transfer heat from the liquid coolant to the surrounding environment (Figure 7a).

To accommodate the rotation of the track links around the frame, the water loop incorporates a live swivel and a 16-spout manifold. The live swivel maintains a watertight seal while allowing rotational freedom between the frame and manifold. Water is distributed to each link through this system. A rubber O-ring ensures sealing, and a set of ball bearings supports rotation while limiting axial movement. An exploded view of the water distribution system is shown in Figure 7b.

3.1.3. Track Link and Components The individual track links that form the robot's drive track are equipped with a full adhesion effector system, similar to the standalone units used in previous ice adhesion tests. Each link integrates an adhesion pad, Peltier element, and heat sink, as well as a mechanical switch to control the direction of current flow through the Peltier

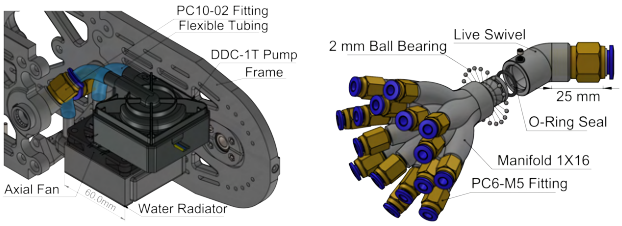

(a) (b)

FIGURE 7: LIQUID COOLING SYSTEM INTEGRATED IN ROBOT PAYLOAD; (A) HEAT DISSIPATION PARTS, (B) WATER MANIFOLD WITH INTEGRATED LIVE SWIVEL

Figure 8 highlights the key components of the track link. Component (1), the *track link top*, secures the *aluminum adhesion pad* (2) to the *TEC1-06308 Peltier element* (3). The Peltier element is thermally interfaced with the *heat sink* (4), which is embedded in a cavity within the *track link bottom* (6). This bottom component also houses internal water channels that direct coolant flow from the *push-in pneumatic coupling* (5) beneath the heat sink. The track links are joined by a *connecting rod* (7), which not only forms the mechanical chain but also enables torque transfer from the drive sprocket. A modified *Double-Pole Double-Throw*

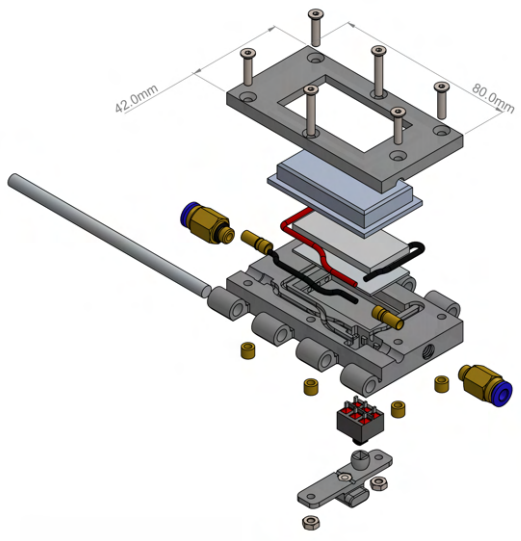

FIGURE 8: EXPLODED VIEW OF THE TRACK LINK AND COMPONENTS.

(DPDT) switch (8) is installed to act as a mechanical H-bridge, controlling the polarity of the current through the Peltier element to toggle between heating and cooling modes. Both the *track link top* and *bottom* are produced using additive manufacturing. The fully assembled track link is shown in Figure 9.

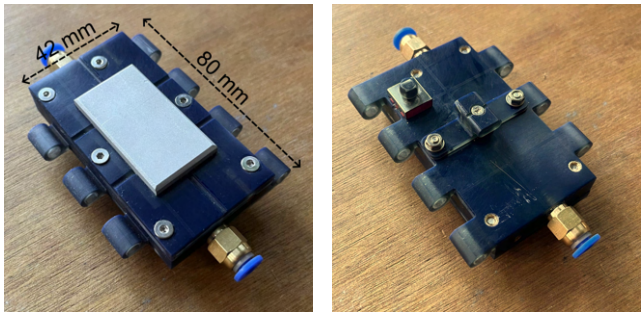

(a) **(b)**

FIGURE 9: ASSEMBLED TRACK LINK; (A) TOP VIEW, (B) BOTTOM VIEW

3.1.4. Track Link Control Precise control of the heating and cooling phases of each track link is essential to ensure timely attachment and detachment from the ice. To achieve this, a passive mechanical control system is implemented that takes advantage of the track's predictable motion around the robot frame. Since each link follows a fixed trajectory, its position along the path can be mapped to a repeatable time sequence, as shown in figure 10. This enables the use of mechanically actuated switches placed at specific points along the frame.

Each track link contains a double-pole double-throw (DPDT) switch, wired as an H-bridge circuit, to control the polarity of the current through the Peltier element, see figure 11. These switches reverse the direction of heat flow, enabling either cooling (to adhere) or heating (to release). The DPDT switches are mechanically actuated via a cam-follower principle, where guides

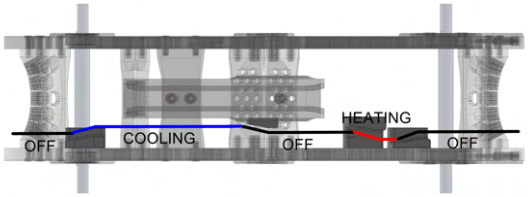

FIGURE 10: COOLING AND HEATING CYCLE ALONG THE ROBOT FRAME.

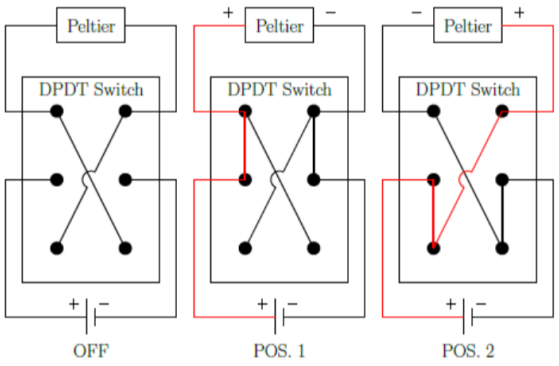

FIGURE 11: DPDT SWITCH WIRED AS MECHANICAL H-BRIDGE SWITCH.

embedded in the robot frame interact with the switch at precise positions in the track's cycle. This approach minimizes the need for complex electronics while ensuring deterministic timing for each adhesion cycle.

3.2. Robot Climbing and Inversion Tests

The finished system, shown in figure 12, is capable of moving at speeds up to 80 cm/min. A 12 VDC, 6.5 W, 36 mm DC planetary geared motor (Model NFP-GA36Y-3525) with a built-in gear reduction ratio of 721:1 was selected as the primary drive unit. This motor delivers a rated torque of 2.75 Nm. An additional 3:1 bevel gear reduction stage further amplifies output torque, enabling the robot to climb steep vertical surfaces.

The robot's climbing ability was evaluated on ice blocks oriented at various inclinations. Experimental results show that the robot can reliably move at speeds up to 65 cm/min on surfaces inclined up to 60°, as shown in the middle panel of Figure 12. At steeper angles, backward tilting reduces the contact effectiveness between the track links and the ice, impairing adhesion. The maximum traveling speed for this tracked robotic climber is limited by the time-to-adhere, which depends on multiple factors such as cooling power, the temperature of the ice and environment, and the temperature of the adhesion pad before contact. Optimizing these parameters enables faster travel. Additional tests revealed that the robot can also hang upside down once proper adhesive contact is established (right panel of Figure 12), demonstrating secure grip and operational flexibility. A video of the robot climbing on an inclined surface can be found at the following link: Robot Climbing Test.

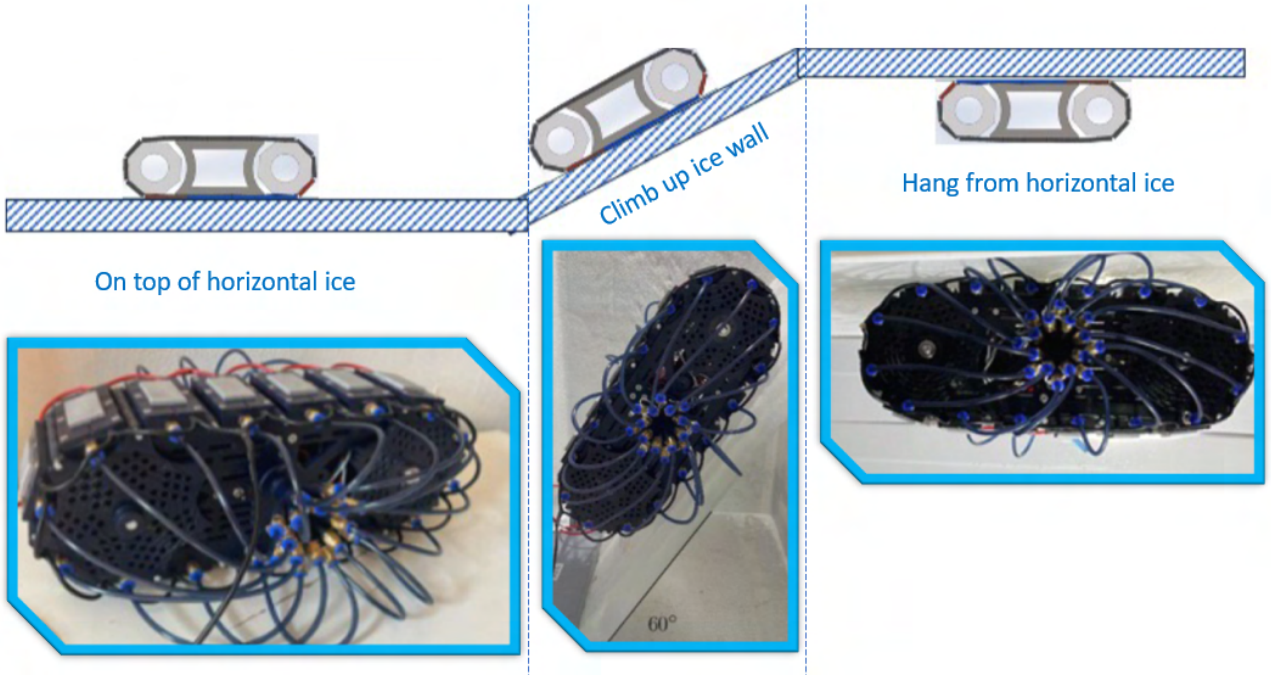

FIGURE 12: CLIMBING TESTS SHOWING THE ROBOT TRAVERSING INCLINED SURFACES UP TO 60° AND HANGING UPSIDE-DOWN FROM ICE AFTER ADHESION.

4. DISCUSSION

The adhesion tests revealed notable differences between the surface treatments. Surprisingly, the increased effective contact area of the grid-patterned adhesion pads did not lead to higher adhesion forces. This suggests that adhesion strength in this system is not dominated by total area alone, but rather by stress distribution and defect tolerance at the interface. The sharp corners and intersecting grooves of the milled grid pattern likely act as stress concentrators; promoting localized stress risers where micro cracks can initiate, potentially leading to premature adhesive or cohesive failure.

In contrast, the polished pads have smooth, deformation-free surfaces, reducing the likelihood of such stress risers forming across the contact area. However, the sharp outer edges left by the polishing process may still act as points of weakness. Grit-blasted surfaces appear to strike a favorable balance: they introduce moderate, isotropic surface roughness that enhances wettability and distributes stress more evenly across the interface. Moreover, the grit-blasting process naturally rounds off sharp pad edges, which may further reduce the probability of crack initiation at the contact boundary. These observations suggest that moderate surface roughness with reduced edge sharpness may be more effective than maximizing contact area when designing for ice adhesion under tensile loading.

This robotic prototype was developed as a potential exploration tool for accessing the subsurface ocean through surface cracks on Enceladus. Although our preliminary tests demonstrate the feasibility of adhesion-based locomotion on icy surfaces, all experiments were carried out under Earth conditions: atmospheric pressure, standard gravity, and temperatures down to $-15°C$.

However, Enceladus presents a vastly different environment. Surface temperatures may drop to $-200°C$, and crevasse pressures are estimated to range between 6 mbar and less than 1 mbar [16]. Although recent studies indicate that the pressure could be higher [17] due to the exsolution and expansion of dissolved gases from ascending water. These conditions would significantly alter the adhesion dynamics of our system, which relies on local melting and refreezing. In these low-pressure environments, the phase diagram of water indicates that heating water ice initiates sublimation; a transition between the solid and liquid phases is not possible. This potentially renders the adhesion mechanism ineffective.

One possible solution is to locally increase the pressure around the adhesion interface by enclosing the links in a sealed cap. In this configuration, sublimation increases the local vapor pressure within the sealed cap, raising it above the triple point and thereby allowing local melting.

The presence of impurities (e.g., minerals) in the ice could reduce the efficiency of freezing and adhesion. We expect that at high concentrations, such impurities may render the adhesion mechanism ineffective. However, if the impurities are in the form of volatiles, we expect them to sublimate as the ice heats up, thereby not hindering the freezing and adhesion processes. As part of future work, we plan to test the adhesion system under simulated low-pressure environments, low-density ice surfaces, and with introduced impurities to evaluate its performance under Enceladus-like conditions.

Additionally, temperature plays a critical role in determining the mechanical properties of ice, including its shear and compressive strength [18]. Testing the adhesion effector at much lower temperatures will help quantify performance losses and guide

system optimization.

These environmental constraints also raise critical questions about power supply and mission duration for exploring icy moons. Assuming a traveling speed of 65 cm/min and an ice thickness of 1–5 km, the robot would take 30–130 hours to reach the subsurface ocean. No current battery can operate reliably for that duration under cryogenic conditions.

Solar power is not viable due to low irradiance at Enceladus's south pole and the shadowed environment within the crevasse. Radioisotope Thermoelectric Generators offer long-term power (2–5 W/kg) and is suitable for a surface lander, but a climbing robot would likely require a tethered power supply.

Compared to other robotic concepts proposed for exploring Enceladus, our robot offers distinct advantages and trade-offs. NASA's IceWorm [12] uses motorized ice screws for anchoring, which are energy-intensive and may induce structural failure due to high local stresses in low density, brittle ice. In contrast, our lightweight design relies on local phase-change adhesion, minimizing stress and potentially improving energy efficiency. NASA's EELS robot [10], a snake-like system for versatile terrain navigation, offers high mobility but involves greater mechanical complexity and higher failure risk. Our track-based robot simplifies mechanical components while enabling reliable, continuous locomotion.

Melting probes [4, 5, 8] can penetrate deep ice layers efficiently but lack surface maneuverability and adaptability once deployed. Our robot concept provides flexible navigation across icy terrain and controlled descent into crevasses, presenting a complementary alternative for missions requiring both surface and near-subsurface access.

Beyond Enceladus, the system could be adapted for lunar missions. The Moon's south pole contains permanently shadowed regions expected to harbor water ice [19, 20]. NASA, ESA, and other space agencies plan to deploy rovers and crewed missions to investigate these regions. Our adhesion system could potentially be integrated into lightweight exploration platforms such as the Lunar Zebro nanorovers [21], enabling access to rugged, ice-rich terrains with minimal infrastructure.

5. CONCLUSIONS

Robotic locomotion on icy surfaces remains a significant challenge but also presents a critical opportunity for both space and terrestrial exploration. In this work, we designed a novel switchable ice adhesion actuator and demonstrated its feasibility through cold chamber experiments. The actuator's performance was evaluated across a variety of end-effector configurations, highlighting how surface finish and texturing influence mechanical interlocking with the ice.

One limitation of the system is its dependence on ice properties, which are affected by environmental factors such as temperature and pressure. Despite this, the actuator was successfully integrated into a modular track-based locomotion platform, demonstrating reliable operation in a lab setting and offering promising performance under extreme conditions.

The robot's modularity, achieved through identical track links and minimal electronic components, allows for flexible configurations and enhances resilience in cold environments. The system can be scaled by increasing the number of links or adapted to carry heavier payloads by switching to a dual-track configuration.

Future work will focus on scaling the system for deployment in real-world rescue operations and further refining the design for extraterrestrial use. Challenges such as power supply, thermal management, and subglacial communication must also be addressed. Ultimately, this robotic platform could support scientific missions in the search for extraterrestrial life or assist in reaching otherwise inaccessible regions on Earth, including glaciers, crevasses, arctic ravines, or hazardous terrain.

ACKNOWLEDGMENT

We thank the Delft Bioengineering Institute (Delft University of Technology) for supporting and sponsoring this project through the BioDate 2020 initiative.

REFERENCES

[1] Porco, C. C., Helfenstein, P., Thomas, P. C., Ingersoll, A. P., Wisdom, J., West, R., Neukum, G., Denk, T., Wagner, R., Roatsch, T., Kieffer, S., Turtle, E., McEwen, A., Johnson, T. V., Rathbun, J., Veverka, J., Wilson, D., Perry, J., Spitale, J., Brahic, A., Burns, J. A., DelGenio, A. D., Dones, L., Murray, C. D. and Squyres, S. "Cassini Observes the Active South Pole of Enceladus." *Science* Vol. 311 No. 5766 (2006): pp. 1393–1401. DOI 10.1126/science.1123013. URL https://www.science.org/doi/10.1126/science.1123013.

[2] Spencer, John R., Barr, Amy C., Esposito, Larry W., Helfenstein, Paul, Ingersoll, Andrew P., Jaumann, Ralf, McKay, Christopher P., Nimmo, Francis and Waite, J. Hunter. "Enceladus: An Active Cryovolcanic Satellite." *Saturn from Cassini-Huygens*. Springer Netherlands, Dordrecht (2009): pp. 683–724. DOI 10.1007/978-1-4020-9217-6_21. URL http://link.springer.com/10.1007/978-1-4020-9217-6_21.

[3] Postberg, F., Clark, R. N., Hansen, C. J., Coates, A. J., Dalle Ore, C. M., Scipioni, F., Hedman, M. M. and Waite, J. H. "Plume and Surface Composition of Enceladus." *Enceladus and the Icy Moons of Saturn*. The University of Arizona Press (2018): pp. 129–162. DOI 10.2458/azu_uapress_9780816537075-ch007. URL https://uapress.arizona.edu/book/enceladus-and-the-icy-moons-of-saturn.

[4] Konstantinidis, Konstantinos, Flores Martinez, Claudio L., Dachwald, Bernd, Ohndorf, Andreas, Dykta, Paul, Bowitz, Pascal, Rudolph, Martin, Digel, Ilya, Kowalski, Julia, Voigt, Konstantin and Förstner, Roger. "A lander mission to probe subglacial water on Saturns moon Enceladus for life." *Acta Astronautica* Vol. 106 (2015): pp. 63–89. DOI 10.1016/j.actaastro.2014.09.012. URL https://linkinghub.elsevier.com/retrieve/pii/S0094576514003610.

[5] Dachwald, Bernd, Mikucki, Jill, Tulaczyk, Slawek, Digel, Ilya, Espe, Clemens, Feldmann, Marco, Francke, Gero, Kowalski, Julia and Xu, Changsheng. "IceMole: a maneuverable probe for clean in situ analysis and sampling of subsurface ice and subglacial aquatic

ecosystems." *Annals of Glaciology* Vol. 55 No. 65 (2014): pp. 14–22. DOI 10.3189/2014AOG65A004. URL https://www-cambridge-org.tudelft.idm.oclc.org/core/journals/annals-of-glaciology/article/icemole-a-maneuverable-probe-for-clean-in-situ-analysis-and-sampling-of-subsurface-ice-and-subglacial-aquatic-ecosystems/A5174FD249A0CB4E8DFBE7B1935E1765.

[6] Ono, Masahiro, Mitchel, Karl, Parness, Aaron, Carpenter, Kalind, Iacoponi, Saverio, Simonson, Ellie, Curtis, Aaron, Ingham, Mitch, Budney, Charles, Estlin, Tara, Parcheta, Carolyn, Detry, Renaud, Nash, Jeremy, de la Croix, Jean-Pierre, Kawata, Jessie and Hand, Kevin. "Enceladus Vent Explorer Concept." *Outer Solar System*. Springer International Publishing, Cham (2018): pp. 665–717. DOI 10.1007/978-3-319-73845-113. URL http://link.springer.com/10.1007/978-3-319-73845-113.

[7] Mousis, O., Bouquet, A., Langevin, Y., André, N., Boithias, H., Durry, G., Faye, F., Hartogh, P., Helbert, J., Iess, L., Kempf, S., Masters, A., Postberg, F., Renard, J. B., Vernazza, P., Vorburger, A., Wurz, P., Atkinson, D. H., Barabash, S., Berthomier, M., Brucato, J., Cable, M., Carter, J., Cazaux, S., Coustenis, A., Danger, G., Dehant, V., Fornaro, T., Garnier, P., Gautier, T., Groussin, O., Hadid, L. Z., Ize, J. C., Kolmasova, I., Lebreton, J. P., Le Maistre, S., Lellouch, E., Lunine, J. I., Mandt, K. E., Martins, Z., Mimoun, D., Nenon, Q., Muñoz Caro, G. M., Rannou, P., Rauer, H., Schmitt-Kopplin, P., Schneeberger, A., Simons, M., Stephan, K., Van Hoolst, T., Vaverka, J., Wieser, M. and Wörner, L. "Moonraker: Enceladus Multiple Flyby Mission." *Planetary Science Journal* Vol. 3 No. 12 (2022): 268. DOI 10.3847/PSJ/ac9c03. URL 2211.00721.

[8] Wilcox, Brian H., Carlton, Jason A., Jenkins, Justin M. and Porter, Fletcher A. "A deep subsurface ice probe for Europa." *IEEE Aerospace Conference Proceedings* (2017)DOI 10.1109/AERO.2017.7943863.

[9] Villanueva, G. L., Hammel, H. B., Milam, S. N., Kofman, V., Faggi, S., Glein, C. R., Cartwright, R., Roth, L., Hand, K. P., Paganini, L., Spencer, J., Stansberry, J., Holler, B., Rowe-Gurney, N., Protopapa, S., Strazzulla, G., Liuzzi, G., Cruz-Mermy, G., El Moutamid, M., Hedman, M. and Denny, K. "JWST molecular mapping and characterization of Enceladus' water plume feeding its torus." *Nature Astronomy* Vol. 7 (2023): pp. 1056–1062. DOI 10.1038/s41550-023-02009-6. URL 2305.18678.

[10] Carpenter, Kalind, Thoesen, Andrew, Mick, Darwin, Martia, Justin, Cable, Morgan, Mitchell, Karl, Hovsepian, Sarah, Jasper, Jay, Georgiev, Nikola, Thakker, Rohan, Kourchians, Ara, Wilcox, Brian, Yip, Michael and Marvi, Hamid. "Exobiology Extant Life Surveyor (EELS)." *Earth and Space 2021*: pp. 328–338. 2021. American Society of Civil Engineers, Reston, VA. DOI 10.1061/9780784483374.033. URL http://ascelibrary.org/doi/10.1061/9780784483374.033.

[11] Konstantinidis, Kostas, Adler, Julian, Thies, Manuel and Förstner, Roger. "Simulation of precise and safe landing near a plume source on Enceladus." *IEEE Aerospace Conference Proceedings* Vol. 2018-March (2018): pp. 1–15. DOI 10.1109/AERO.2018.8396476.

[12] Curtis, Aaron, Martone, Matt and Parness, Aaron. "Roving on ice: Field testing an Ice Screw End Effector and sample collection tool." *IEEE Aerospace Conference Proceedings* Vol. 2018-March (2018): pp. 1–17. DOI 10.1109/AERO.2018.8396715.

[13] Ryzhkin, Ivan A. and Petrenko, Victor F. "Physical mechanisms responsible for ice adhesion." *Journal of Physical Chemistry B* Vol. 101 No. 32 (1997): pp. 6267–6270. DOI 10.1021/JP9632145/ASSET/IMAGES/MEDIUM/JP9632145E00000 URL https://pubs-acs-org.tudelft.idm.oclc.org/doi/full/10.1021/jp9632145.

[14] Chen, Jing, Liu, Jie, He, Min, Li, Kaiyong, Cui, Dapeng, Zhang, Qiaolan, Zeng, Xiping, Zhang, Yifan, Wang, Jianjun and Song, Yanlin. "Superhydrophobic surfaces cannot reduce ice adhesion." *Applied Physics Letters* Vol. 101 No. 11 (2012): p. 111603. DOI 10.1063/1.4752436. URL https://aip-scitation-org.tudelft.idm.oclc.org/doi/abs/10.1063/1.4752436.

[15] Makkonen, Lasse. "Ice adhesion - Theory, measurements and countermeasures." *Journal of Adhesion Science and Technology* Vol. 26 No. 4-5 (2012): pp. 413–445. DOI 10.1163/016942411X574583.

[16] Schmidt, Jürgen, Brilliantov, Nikolai, Spahn, Frank and Kempf, Sascha. "Slow dust in Enceladus' plume from condensation and wall collisions in tiger stripe fractures." *Nature* Vol. 451 No. 7179 (2008): pp. 685–688. DOI 10.1038/nature06491. URL http://www.nature.com/articles/nature06491.

[17] Mitchell, Karl L., Rabinovitch, Jason, Scamardella, Jonathan C. and Cable, Morgan L. "A Proposed Model for Cryovolcanic Activity on Enceladus Driven by Volatile Exsolution." *Journal of Geophysical Research: Planets* Vol. 129 No. 7 (2024): p. e2023JE007977. DOI https://doi.org/10.1029/2023JE007977. URL https://agupubs.onlinelibrary.wiley.com/doi/pdf/10.1029/2023JE007977, URL https://agupubs.onlinelibrary.wiley.com/doi/abs/10.1029/2023JE007977. E2023JE007977 2023JE007977.

[18] Colgan, William and Arenson, Lukas. "Open-Pit Glacier Ice Excavation: Brief Review." *Journal of Cold Regions Engineering* Vol. 27 (2013): pp. 223–243. DOI 10.1061/(ASCE)CR.1943-5495.0000057.

[19] Brown, H.M., Boyd, A., Denevi, B.W., Henriksen, M.R., Manheim, Madeleine, Robinson, M.S., Speyerer, E.J. and Wagner, Robert. "Resource potential of lunar permanently shadowed regions." *Icarus* Vol. 377 (2022): p. 114874. DOI 10.1016/j.icarus.2021.114874.

[20] Lemelin, Myriam, Li, Shuai, Mazarico, Erwan, Siegler, Matthew A., Kring, David A. and Paige, David A. "Framework for Coordinated Efforts in the Exploration of Volatiles in the South Polar Region of the Moon." *The Planetary Science Journal* Vol. 2 No. 3 (2021): p. 103. DOI 10.3847/PSJ/abf3c5. URL https://dx.doi.org/10.3847/PSJ/abf3c5.

[21] Muñoz Tejeda, J. M., Morón Montesdeoca, D., Verma, M. K., Fajardo Peña, P. and Verhoeven, C. "Environmental

analysis of nanorovers in a swarm for lunar scientific missions." 2019. URL http://www.iafastro.org/publications/iac-papers/. 70th International Astronautical Congress, IAC 2019, IAC 2019 ; Conference date: 21-10-2019 Through 25-10-2019.